

Schottky-Barrier-Free Contacts with Two-Dimensional Semiconductors by Surface-Engineered MXenes

Yuanyue Liu,^{*,†,‡,§} Hai Xiao,^{†,§} and William A. Goddard, III^{*,†,§}[†]Materials and Process Simulation Center, [‡]The Resnick Sustainability Institute, California Institute of Technology, Pasadena, California 91125, United States

Supporting Information

ABSTRACT: Two-dimensional (2D) metal carbides and nitrides, called MXenes, have attracted great interest for applications such as energy storage. We demonstrate their potential as Schottky-barrier-free metal contacts to 2D semiconductors, providing a solution to the contact-resistance problem in 2D electronics. On the basis of first-principles calculations, we find that the surface chemistry strongly affects Fermi level of MXenes: O termination always increases the work function with respect to that of bare surface, OH always decreases it, whereas F exhibits either trend depending on the specific material. This phenomenon originates from the effect of surface dipoles, which together with the weak Fermi level pinning, enable Schottky-barrier-free hole (or electron) injection into 2D semiconductors through van der Waals junctions with some of the O-terminated (or all the OH-terminated) MXenes. Furthermore, we suggest synthetic routes to control surface terminations based on calculated formation energies. This study enhances understanding of the correlation between surface chemistry and electronic/transport properties of 2D materials, and also gives predictions for improving 2D electronics.

The MXenes are a class of two-dimensional (2D) metal carbides/nitrides that have the general formula of $M_{n+1}X_nT_x$ (M is an early transition metal, X is C and/or N, T represents a surface terminating group, and $n = 1-3$).¹⁻³ They are usually produced by selective etching of the A element layer from the bulk $M_{n+1}AX_n$ phases⁴ (A = Al, Si etc.), using strong etching solutions such as HF or a mixture of HCl and LiF.^{1,2,5} This process leads to T = O, OH, and/or F. The layers are then exfoliated by sonication.^{1,2,5} MXenes have already shown a great potential in batteries,⁶⁻⁹ capacitors,^{5,10,11} and water treatment.^{12,13}

Many MXenes have excellent electrical conductivity, which benefits their use as electrodes in electrochemical systems.^{1,2} We demonstrate their potential as Schottky-barrier-free metal contacts to 2D semiconductors. Although electronics based on 2D semiconductors (e.g., transition metal dichalcogenides, black phosphorus) have attracted interest, their development is significantly hindered by the large Schottky barrier (SB) at the metal–semiconductor junction (MSJ).¹⁴⁻¹⁶ The use of Ti_2CT_x as electrodes for 2D MoS_2 and WSe_2 field effect transistors have been experimentally demonstrated, yet with significant SBs.¹⁷ We predict SB-free contacts can be achieved by using MXenes with proper surface terminations, which form van der Waals (vdW)

junctions^{16,18,19} with 2D semiconductors. We also suggest synthetic routes to control the surface termination based on calculated formation energies.

We focus here on MXenes that have been experimentally realized or have available $M_{n+1}AX_n$ precursors.⁴ We performed density functional theory calculations using the Vienna Ab-initio Simulation Package (VASP)^{20,21} with projector augmented wave pseudopotentials^{22,23} and the Perdew–Burke–Ernzerhof (PBE) exchange–correlation functional.²⁴ In some cases, we also used the B3PW91 hybrid functional²⁵ (which is more accurate but computationally expensive) for comparison. The London Dispersion (vdW attraction) interactions in the heterojunction are corrected using the empirical D3 method.²⁶ We used 400 eV for the plane-wave cutoff, and fully relaxed the systems until the final force on each atom was less than 0.01 eV/Å.

Figure 1b shows a representative structure of an MXene. The M and X layers alternate following ABC close packing, and T prefers

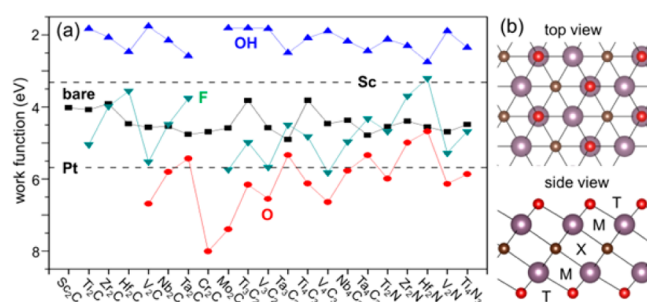


Figure 1. (a) Work functions of MXenes with various terminations. Bare surface, black square; O termination, red circle; OH, blue up-triangle; F, cyan down-triangle. For comparison, work functions of Sc and Pt metal are indicated by dashed lines. (b) Atomic structure of a representative M_2XT_2 . M, purple; X, gray; T, red.

to be on the *fcc* site of the surface to maximize the coordination with M (the exceptions are group 6 MXenes, Cr_2CT_x and Mo_2CT_x , whose stacking depends on T; see SI for details). We first consider all surface sites are occupied by one type of T (mixed T discussed later). Figure 1a shows the calculated work function (*W*) for various MXenes. Note some of them are semiconductors (Sc_2CO_2 , $Sc_2C(OH)_2$, Sc_2CF_2 , Ti_2CO_2 , Hf_2CO_2 , Zr_2CO_2 , $Cr_2C(OH)_2$, and Cr_2CF_2), the *W* of which is not an intrinsic property but rather depends on the doping and hence is not

Received: October 17, 2016

Published: November 22, 2016

shown. The W of some of the MXenes has been calculated (ref 27), which agrees with our results. We find that W is sensitive to T: compared with bare surface, O termination always increases W , OH always decreases W , whereas F exhibits either trend depending on the specific material.

Interestingly, all the OH terminated MXenes have a rather low W , even lower than that of Sc metal, which has been reported to have a small SB with multilayer MoS₂.²⁸ Some of the O terminated MXenes have a rather high W , even higher than that of Pt metal, which has the highest W among the elemental metals. The W of F terminated MXenes (W_F) always falls between the corresponding W_O and W_{OH} . In addition, we observe a positive correlation between W_F and W_O , but a negative correlation between W_{OH} and W_O . These correlations become clear in Figure 2a, where W_F and W_{OH} are plotted against W_O .

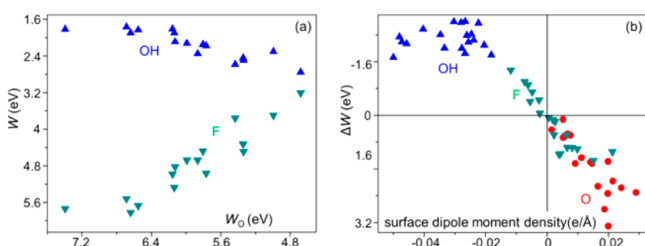


Figure 2. (a) Work function of OH and F terminated MXenes as function of work function of O terminated MXenes. (b) Work function variation induced by surface termination, as function of surface dipole moment density.

To understand these observations, we partition the W of a T terminated MXene (W_T) as

$$W_T = W_{\text{bare}} + \Delta W = W_{\text{bare}} + C \cdot \Delta D_s + \Delta E_F \quad (1)$$

where ΔW is the change in W with respect to that of bare surface (W_{bare}), ΔD_s is the change of surface dipole moment density induced by T, C is a constant, and ΔE_F is the Fermi level shift due to chemical bonding between T and M. The ΔD_s is generally defined as

$$\Delta D_s = \int_{z_1}^{z_2} \int \int \Delta \rho(x, y, z) dx dy / S \quad (2)$$

where $\Delta \rho$ is the change of charge density (including ions that can be treated as point charges) induced by T, z is the coordinate normal to the surface, and S is the surface area. $\Delta \rho$ gradually approaches zero when going away from the surface deep into the bulk or vacuum, at which points z_1 and z_2 are chosen. However, for atomically thin MXenes, z_1 is not well-defined because of the nonzero $\Delta \rho$ in the bulk (see Figure S1). This invalidates the use of eq 2. Albeit this ambiguity, the dipole effect can still be approximated by the dipole moment density of the MXene with only one side of the surfaces terminated, which we calculate as

$$\Delta D_s \sim D_s = \int_{z_1}^{z_2} \int \int \rho(x, y, z) dx dy / S$$

where z_1 and z_2 are chosen at the points where $\rho = 0$ (i.e., deep into vacuum).

Figure 2b plots the ΔW as a function of D_s . We find ΔW always has the same sign as D_s , suggesting D_s controls the decrease or increase of W . Specifically, O termination always leads to a positive D_s (i.e., the negative end of the dipole points to T), OH termination always results in a negative D_s , whereas F can have either positive or negative D_s depending on the specific material.

Indeed, this matches well with the decrease or increase in W . Note the surface OH group has a dipole moment ~ -0.33 eÅ with O pointing to the M, which is compensated by an opposite dipole due to charge redistribution induced by OH adsorption; nevertheless, the net dipole moment is still negative. We also note that the negative dipole of F termination for some materials does not mean F carries positive charge. As shown by the electron density change in Figure S1, after F adsorption, the surface M layer transfers electrons to both F and the underneath X layer; however, X gets more electrons than T, resulting in a negative dipole even when F is negatively charged. Compared with F, O tends to get more electrons to saturate the two unpaired p orbitals. The amount of electron transfer from M to O is greater than that to X, thus the O induced dipole is always positive. These arguments explain well the relationships between surface termination and the W change as mentioned above.

More quantitatively, for O or F terminated MXenes, the magnitudes of ΔW and D_s exhibit a quasi-linear correlation, but for OH there is no clear correlation. A similar observation has been reported in ref 27. This is probably due to the complexity of the OH terminated surface, where the dipole is contributed by both the OH group and the adsorption-induced charge redistribution. In addition, the ΔE_F can vary with M, reducing the correlation between ΔW and D_s .

The high/low W of some of the MXenes suggests they have the potential of injecting carriers into 2D semiconductors. One of the most important parameters that determine the resistance to carrier injection is Schottky barrier height (Φ), which is defined as the energy difference between the Fermi level and the band edge of the semiconductor in the MSJ:

$$\Phi_e = E_{\text{CBM}} - E_F, \quad \Phi_h = E_F - E_{\text{VBM}} \quad (3)$$

where Φ_e and Φ_h are the Schottky barrier heights for electrons and holes, respectively; CBM denotes the conduction band minimum of the semiconductor, and VBM denotes the valence band maximum. To reduce the contact resistance and improve device performance, Φ_e (for electron injection) or Φ_h (for hole injection) needs to be as low as possible (a SB-free contact is achieved when Φ becomes zero or negative). For a defect-free MSJ, neglecting the interaction between the metal and the semiconductor, eq 3 becomes

$$\Phi_e = E_{\text{CBM}}^0 + W, \quad \Phi_h = -W - E_{\text{VBM}}^0 \quad (4)$$

where E_{CBM}^0 and E_{VBM}^0 are the CBM and VBM energies of the semiconductor in a vacuum. Therefore, a low/high W is beneficial for electron/hole injection. Although eq 4 provides general guidance for comparing Φ , the metal–semiconductor interaction usually causes deviations of eq 4 from eq 3,²⁹ thus the accurate assessment of Φ requires explicit modeling or measurement of the heterogeneous MSJ.

Figure 3a shows a MSJ with Hf₂N(OH)₂ on top of WSe₂. These two materials have a small lattice mismatch of <3%, thus the primitive cells (marked by arrows) are used for calculation. To determine the band edge positions of semiconductor in the MSJ, we analyze the character of the electronic state by projecting its wave function onto each atom (this method has been widely used for studying SB^{30,31}). The WSe₂ contribution to the state is reflected by the color of the circle in the band structure. We find the Fermi level of the MSJ is above the CBM (confirmed by the charge density distribution), showing a negative Φ_e , i.e., electrons are spontaneously transferred from Hf₂N(OH)₂ to the conduction band of WSe₂ upon contact. Note that Figure 3a is calculated using PBE functional (with D3 method for vdW

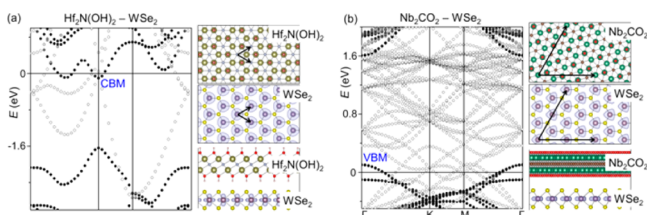


Figure 3. Band structures (left) and atomic structures (right) for (a) $\text{Hf}_2\text{N}(\text{OH})_2$ - WSe_2 junction and (b) Nb_2CO_2 - WSe_2 junction. The Fermi level is set to zero. The WSe_2 contribution to the electronic state is represented by the blackness of the circle interior (i.e., full black means state is purely from WSe_2 , full white indicates state is purely from MXene, whereas gray suggests state is hybridized between WSe_2 and MXene). The charge density distributions of WSe_2 CBM in the $\text{Hf}_2\text{N}(\text{OH})_2$ - WSe_2 junction and WSe_2 VBM in the Nb_2CO_2 - WSe_2 junction are displayed by the light-blue iso-surfaces on the right. The arrows show periodic cells that are overlaid in the junctions.

correction), which is known to underestimate the band gap. To check whether this affects the Φ_e , we recalculated the electronic structure using B3PW91 hybrid functional, which generally gives much more accurate band gaps^{32,33} as well as band offsets.³⁴ As shown in the SI, the Φ_e remains negative (−0.10 eV for PBE vs −0.12 eV for B3PW91). Therefore, we conclude that $\text{Hf}_2\text{N}(\text{OH})_2$ spontaneously injects electrons into WSe_2 upon contact. Because WSe_2 has the highest CBM among the commonly studied 2D semiconductors (molybdenum/tungsten dichalcogenides and black phosphorus),^{35,36} whereas $\text{Hf}_2\text{N}(\text{OH})_2$ has the highest W among OH terminated MXenes (Figure 1a), we expect all the OH terminated MXenes can form SB-free contacts for electron injection into these common 2D semiconductors.

Figure 3b shows a MSJ with Nb_2CO_2 on top of WSe_2 . These two materials have a large lattice mismatch of >5%, thus we used a supercell (marked by arrows) for calculation to minimize the strain. Analogous to the above case, we find the Fermi level is below the VBM of the semiconductor in the MSJ, showing a negative Φ_h , i.e., holes are spontaneously transferred from Nb_2CO_2 to the valence band of WSe_2 upon contact. The negative Φ_h is confirmed by using the B3PW91 hybrid functional to recalculate the electronic structure (−0.10 eV for PBE vs −0.08 eV for B3PW91; see SI). We note many other O-terminated MXenes have a W higher than that of Nb_2CO_2 , so they can also be expected to exhibit even more negative Φ_h . In addition, the spin-orbit coupling (SOC) further increases the VBM³⁵ and hence reduce the Φ_h (similarly, the SOC generally decreases the CBM and thus also reduce the Φ_e ; whereas for 2D transition metal dichalcogenides, the SOC has negligible effect on the CBM position³⁵). Therefore, we conclude SB-free contacts for hole injection into WSe_2 can be formed by using Nb_2CO_2 , V_2CO_2 , Cr_2CO_2 , Mo_2CO_2 , $\text{Ti}_3\text{C}_2\text{O}_2$, $\text{V}_3\text{C}_2\text{O}_2$, $\text{Ti}_4\text{C}_3\text{O}_2$, $\text{V}_4\text{C}_3\text{O}_2$, Ti_2NO_2 , V_2NO_2 , and $\text{Ti}_4\text{N}_3\text{O}_2$.

The ability to achieve SB-free contacts by using 2D MXenes is due to not only their low/high W of specific materials but also weak vdW interactions between the metal and the semiconductor in the MSJ, which has been shown to reduce the Fermi level pinning effect.¹⁶ This is also observed in our examples: although Nb_2CO_2 and Pt have a similar W (Figure 1a), the Nb_2CO_2 has a negative Φ_e as shown in Figure 3b, whereas the Φ_e for Pt is calculated to be ~ 0.34 eV³⁷ (both cases are calculated at PBE level without SOC), confirming a weaker Fermi level pinning at the vdW MSJ.

In current experiments, MXenes are usually terminated with a mixture of F, O, and OH, due to the use of aqueous F-containing

solution for etching. The mix of O and OH at the surface brings the W back into an intermediate value. Therefore, we consider it best to have only one type dominant. Although in some cases F termination can also lead to a low/high W (e.g., Mo_2CF_2 , $\text{V}_3\text{C}_2\text{F}_2$, $\text{V}_4\text{C}_3\text{F}_2$, Hf_2NF_2 ; see Figure 1a), it generally results in a modest W , suggesting that F termination should be suppressed in most cases. Experimentally, it has been shown that using LiF-HCl instead of HF can increase/decrease the ratio of O/F,³⁸ and alkalization treatment can increase the concentration of OH.¹³ We show the preference of different terminations can be further modified by applying an electrochemical potential. The formation free energy (ΔG_T) of T termination with respect to bare surface can be calculated as

$$\Delta G_T = G(\text{M}_{n+1}\text{X}_n\text{T}_2) - G(\text{M}_{n+1}\text{X}_n) - 2G(\text{T})$$

where $G(\text{H}) = 1/2G(\text{H}_2) - eU$, $G(\text{OH}) = G(\text{H}_2\text{O}) - G(\text{H})$, $G(\text{O}) = G(\text{H}_2\text{O}) - 2G(\text{H})$. $G(\text{H}_2)$ and $G(\text{H}_2\text{O})$ are the free energies of H_2 and H_2O at standard condition, respectively, and U is the applied voltage vs the reversible hydrogen electrode (RHE). For simplicity, we assume the system is also in equilibrium with HF at standard condition, thus: $G(\text{F}) = G(\text{HF}) - G(\text{H})$ (note that this assumption overestimates $G(\text{F})$).

Figure 4 shows the calculated ΔG_T at $U = 0$ and 1.23 V, which correspond to the thermodynamic limits for water splitting. We

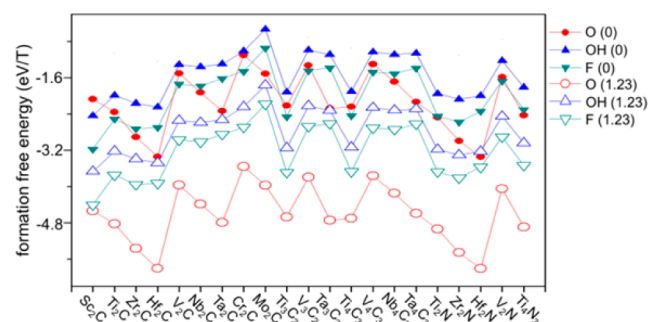


Figure 4. Calculated formation free energies of surface terminations for various MXenes, at $U = 0$ (solid) and 1.23 V (hollow) vs RHE.

find F termination is always more favorable thermodynamically than OH (ΔG_F and ΔG_{OH} exhibit a notable positive correlation), whereas the preference of F vs O depends on the specific material and U . At $U = 1.23$ V, O termination becomes much more favorable than F (>0.8 eV/T; except Sc_2C). This benefits from the stronger dependence of ΔG_O on U compared to ΔG_F , since the adsorption of O involves more charge transfer. Therefore, a high U thermodynamically favors O termination. Starting from O terminated MXenes, one can convert the surface to OH termination by applying a positive U , as the difference between ΔG_O and ΔG_{OH} becomes smaller with increasing U and can be inverted given a high enough U (see SI for assessment of critical U for the case of V_2C). Moreover, treating MXenes with O/H gas or plasma could also modify the surface toward the desired terminations.

There are other benefits of using 2D MXenes as metal electrodes. Because of the atomic thickness, the 2D metals are transparent and flexible,^{39,40} thus they can be integrated into transparent and flexible electronics.^{14,41–43} It also allows for full encapsulation of the device by boron nitride to avoid material contamination/degradation.^{44,45} Moreover, the atomically flat interface between the metal and semiconductor, and the suppression of gap states at the interface due to the weak vdW

interaction,¹⁶ can reduce the charge carrier scattering and recombination, improving performance for electronic and optoelectronic applications. Finally, we point out defects in the semiconductors often create gap states⁴⁶ that lead to Fermi level pinning, and would cause deviation from calculated SB values. However, this effect is similar for different metal contacts. Therefore, it is robust to conclude that, compared with other metals, use of proper MXenes can lower the SB.

In summary, on the basis of first-principles calculations, we demonstrate potential of surface-engineered MXenes as SB-free contacts to 2D semiconductors. Work functions of MXenes show strong dependence on surface termination, which is largely due to the surface dipole effect. When vdW contact is formed with 2D semiconductors, some of O terminated MXenes can spontaneously inject holes, whereas all the OH terminated MXenes can spontaneously transfer electrons. We also suggest synthetic routes toward desired surface terminations.

■ ASSOCIATED CONTENT

Supporting Information

The Supporting Information is available free of charge on the ACS Publications website at DOI: 10.1021/jacs.6b10834.

Computational details (PDF)

■ AUTHOR INFORMATION

Corresponding Authors

*Y.L. yuan Yue.liu.microman@gmail.com

*W.A.G. wag@wag.caltech.edu

ORCID

Yuan Yue Liu: 0000-0002-5880-8649

Hai Xiao: 0000-0001-9399-1584

William A. Goddard III: 0000-0003-0097-5716

Notes

The authors declare no competing financial interest.

■ ACKNOWLEDGMENTS

Y.L. thanks support from Resnick Prize Postdoctoral Fellowship at Caltech. This research was funded by DOE DE-SC0014607. This work used computational resources sponsored by the DOE's Office of Energy Efficiency and Renewable Energy and located at the National Renewable Energy Laboratory, the Extreme Science and Engineering Discovery Environment (XSEDE; supported by NSF Grant ACI-1053575), and the National Energy Research Scientific Computing Center (NERSC; a DOE Office of Science User Facility supported by the Office of Science of the U.S. DOE under Contract DE-AC02-05CH11231).

■ REFERENCES

- (1) Lei, J.-C.; Zhang, X.; Zhou, Z. *Front. Phys.* **2015**, *10*, 276.
- (2) Naguib, M.; Mochalin, V. N.; Barsoum, M. W.; Gogotsi, Y. *Adv. Mater.* **2014**, *26*, 992.
- (3) Naguib, M.; Kurtoglu, M.; Presser, V.; Lu, J.; et al. *Adv. Mater.* **2011**, *23*, 4248.
- (4) Eklund, P.; Beckers, M.; Jansson, U.; Högberg, H.; et al. *Thin Solid Films* **2010**, *518*, 1851.
- (5) Ghidui, M.; Lukatskaya, M. R.; Zhao, M.-Q.; Gogotsi, Y.; Barsoum, M. W. *Nature* **2014**, *516*, 78.
- (6) Tang, Q.; Zhou, Z.; Shen, P. *J. Am. Chem. Soc.* **2012**, *134*, 16909.
- (7) Xie, Y.; Naguib, M.; Mochalin, V. N.; Barsoum, M. W.; et al. *J. Am. Chem. Soc.* **2014**, *136*, 6385.
- (8) Naguib, M.; Halim, J.; Lu, J.; Cook, K. M.; et al. *J. Am. Chem. Soc.* **2013**, *135*, 15966.
- (9) Liang, X.; Garsuch, A.; Nazar, L. F. *Angew. Chem., Int. Ed.* **2015**, *54*, 3907.
- (10) Lukatskaya, M. R.; Mashtalir, O.; Ren, C. E.; Dall'Agnese, Y.; et al. *Science* **2013**, *341*, 1502.
- (11) Boota, M.; Anasori, B.; Voigt, C.; Zhao, M.-Q.; et al. *Adv. Mater.* **2016**, *28*, 1517.
- (12) Rasool, K.; Helal, M.; Ali, A.; Ren, C. E.; et al. *ACS Nano* **2016**, *10*, 3674.
- (13) Peng, Q.; Guo, J.; Zhang, Q.; Xiang, J.; et al. *J. Am. Chem. Soc.* **2014**, *136*, 4113.
- (14) Fiori, G.; Bonaccorso, F.; Iannaccone, G.; Palacios, T.; et al. *Nat. Nanotechnol.* **2014**, *9*, 768.
- (15) Allain, A.; Kang, J.; Banerjee, K.; Kis, A. *Nat. Mater.* **2015**, *14*, 1195.
- (16) Liu, Y.; Stradins, P.; Wei, S.-H. *Sci. Adv.* **2016**, *2*, e1600069.
- (17) Xu, J.; Shim, J.; Park, J.-H.; Lee, S. *Adv. Funct. Mater.* **2016**, *26*, 5328.
- (18) Liu, Y.; Weiss, N. O.; Duan, X.; Cheng, H.-C.; et al. *Nature Reviews Materials* **2016**, *1*, 16042.
- (19) Novoselov, K. S.; Mishchenko, A.; Carvalho, A.; Castro Neto, A. H. *Science* **2016**, *353*, aac9439.
- (20) Kresse, G.; Hafner, J. *Phys. Rev. B: Condens. Matter Mater. Phys.* **1993**, *47*, 558.
- (21) Kresse, G.; Furthmüller, J. *Phys. Rev. B: Condens. Matter Mater. Phys.* **1996**, *54*, 11169–11186.
- (22) Kresse, G.; Joubert, D. *Phys. Rev. B: Condens. Matter Mater. Phys.* **1999**, *59*, 1758.
- (23) Blöchl, P. E. *Phys. Rev. B: Condens. Matter Mater. Phys.* **1994**, *50*, 17953.
- (24) Perdew, J. P.; Burke, K.; Ernzerhof, M. *Phys. Rev. Lett.* **1996**, *77*, 3865.
- (25) Becke, A. D. *J. Chem. Phys.* **1993**, *98*, 5648.
- (26) Grimme, S.; Antony, J.; Ehrlich, S.; Krieg, H. *J. Chem. Phys.* **2010**, *132*, 154104.
- (27) Khazaei, M.; Arai, M.; Sasaki, T.; Ranjbar, A.; et al. *Phys. Rev. B: Condens. Matter Mater. Phys.* **2015**, *92*, 075411.
- (28) Das, S.; Chen, H.-Y.; Penumatcha, A. V.; Appenzeller, J. *Nano Lett.* **2012**, *13*, 100.
- (29) Tung, R. T. *Appl. Phys. Rev.* **2014**, *1*, 011304.
- (30) Gong, C.; Colombo, L.; Wallace, R. M.; Cho, K. *Nano Lett.* **2014**, *14*, 1714.
- (31) Kang, J.; Liu, W.; Sarkar, D.; Jena, D.; et al. *Phys. Rev. X* **2014**, *4*, 031005.
- (32) Xiao, H.; Tahir-Kheli, J.; Goddard, W. A. *J. Phys. Chem. Lett.* **2011**, *2*, 212.
- (33) Crowley, J. M.; Tahir-Kheli, J.; Goddard, W. A. *J. Phys. Chem. Lett.* **2016**, *7*, 1198.
- (34) Xiao, H.; Goddard, W. A. *J. Chem. Phys.* **2014**, *141*, 094701.
- (35) Kang, J.; Tongay, S.; Zhou, J.; Li, J.; et al. *Appl. Phys. Lett.* **2013**, *102*, 012111.
- (36) Cai, Y.; Zhang, G.; Zhang, Y.-W. *Sci. Rep.* **2014**, *4*, 6677.
- (37) Wang, Y.; Yang, R. X.; Quhe, R.; Zhong, H. *Nanoscale* **2015**.
- (38) Hope, M. A.; Forse, A. C.; Griffith, K. J.; Lukatskaya, M. R.; et al. *Phys. Chem. Chem. Phys.* **2016**, *18*, 5099.
- (39) Dillon, A. D.; Ghidui, M. J.; Krick, A. L.; Griggs, J.; et al. *Adv. Funct. Mater.* **2016**, *26*, 4162.
- (40) Hantanasirisakul, K.; Zhao, M.-Q.; Urbankowski, P.; Halim, J.; et al. *Adv. Electron. Mater.* **2016**, *2*, 1600050.
- (41) Akinwande, D.; Petrone, N.; Hone, J. *Nat. Commun.* **2014**, *5*, 5678.
- (42) Das, S.; Gulotty, R.; Sumant, A. V.; Roelofs, A. *Nano Lett.* **2014**, *14*, 2861.
- (43) Roy, T.; Tosun, M.; Kang, J. S.; Sachid, A. B.; et al. *ACS Nano* **2014**, *8*, 6259.
- (44) Cui, X.; Lee, G.-H.; Kim, Y. D.; Arefe, G.; et al. *Nat. Nanotechnol.* **2014**, *10*, 534.
- (45) Avsar, A.; Vera-Marun, I. J.; Tan, J. Y.; Watanabe, K.; et al. *ACS Nano* **2015**, *9*, 4138.
- (46) Liu, Y.; Stradins, P.; Wei, S.-H. *Angew. Chem., Int. Ed.* **2016**, *55*, 965.